ISA Transactions 142 (2023) 360–371

Contents lists available at ScienceDirect

ISA Transactions

journal homepage: www.elsevier.com/locate/isatrans

Research article

Lyapunov stability of cable-driven manipulators with synthetic fibre cables regulated by non-linear full-state feedback controller

Lorenzo De Mari Casareto Dal Verme [a,b,*], Daniele Ludovico [b], Alessandro Pistone [b], Carlo Canali [b], Darwin G. Caldwell [b]

[a] Dipartimento di Informatica, Bioingegneria, Robotica e Ingegneria dei Sistemi (DIBRIS), Università di Genova, Via Balbi, 5, Genova, 16126, Italy
[b] Advanced Robotics (ADVR), Istituto Italiano di Tecnologia, Via Morego, 30, Genova, 16163, Italy

ARTICLE INFO

Article history:
Received 13 April 2023
Received in revised form 21 July 2023
Accepted 19 August 2023
Available online 22 August 2023

Keywords:
Control engineering
Full-state feedback control
Lyapunov methods
Cable-driven manipulators
Four elements model

ABSTRACT

Robotic manipulators provide advantages in working environments regarding efficiency and safety, which is further increased in the case of elastic joint manipulators, whose mechanical compliance reduces the energy involved in collisions with workers. Cable-driven manipulators are elastic joint manipulators particularly suitable for industrial inspection thanks to the relocation of actuators outside hostile environments, increasing the manipulator payload-to-weight ratio. Recently, synthetic fibre cables are substituting steel cables due to their better-performing mechanical properties, but their visco-elastic behaviour must be compensated in the controller design. The key novelty of this work is using the four elements model, which includes the viscous behaviour, to design a non-linear full-state feedback controller for cable-driven manipulators. Furthermore, the mathematical proof of the closed-loop Lyapunov stability is provided.

1. Introduction

In recent decades, robotic systems have become increasingly relevant in working environments. Indeed, robots are able to perform a wide variety of different tasks, supporting workers. This growth is occurring because their employment can improve working efficiency, both in terms of time and cost, and can significantly reduce or even eliminate risks to human workers' safety and fatigue [1].

One of the most important robotic applications is manipulation since it enables physical interaction with the environment surrounding the robot. Industrial and manufacturing sectors are the most common environments where robotic manipulators are exploited since, in these contexts, they can commonly lift and place heavy and dangerous objects – like car plates and steel beams – or perform industrial inspection and maintenance tasks in hazardous and harsh environments, avoiding any risks to human lives. Nevertheless, humans must also manipulate in contexts other than industries, e.g. construction sites, medicine, and agriculture. Even in these applications, robotic arms can be a great solution to reach a high level of efficiency, safety, and speed that is impossible for human workers to attain [2–4].

Usually, robotic manipulators are divided into two primary families [5]: rigid manipulators and flexible manipulators, which, in turn, are subdivided into flexible link and elastic joint manipulators.

Elastic joint manipulators have many advantages with respect to rigid joints manipulators, such as improving the robot dynamic efficiency or ensuring high reduction ratios with power-efficient compact inline devices [6]. Moreover, the mechanical compliance provided by elastic actuation or transmission reduces the kinetic energy in any possible collisions reducing the risk of injury to the workers, increasing their safety. However, the task of controlling this kind of manipulators is complicated by the presence of joints elasticity. Indeed, if an elastic joint manipulator is controlled using just the motor driver feedback, the lack of compensation for the joints flexibility may lead to end-effector position and orientation errors under heavy load or high joint torque [7,8]. Boussoffara et al. explained how neglecting joints flexibility can even lead to instability [9]. Thus, when dealing with model-based control of elastic joint manipulators, joints flexibility must be included in the robot model to avoid performance degradation [10]. In 1981, Nicosia et al. presented one of the first studies that considered the elasticity in the dynamic model of a manipulator [11]. In 1987, Spong proposed a Lagrangian formulation that, assuming a large reduction ratio, simplifies the dynamic model of an elastic joint manipulator [12], while, in 2015, Buondonno and De Luca

* Corresponding author at: Dipartimento di Informatica, Bioingegneria, Robotica e Ingegneria dei Sistemi (DIBRIS), Università di Genova, Via Balbi, 5, Genova, 16126, Italy.
E-mail addresses: lorenzo.demaricasareto@iit.it (L. De Mari Casareto Dal Verme), daniele.ludovico@iit.it (D. Ludovico), alessandro.pistone@iit.it (A. Pistone), carlo.canali@iit.it (C. Canali), darwin.caldwell@iit.it (D.G. Caldwell).

https://doi.org/10.1016/j.isatra.2023.08.019

published an efficient generalised Newton–Euler algorithm that computes the inverse dynamics of these robots [13]. Farah et al. exploited a geometrical and dynamic identification procedure to produce a dynamic model that considers the stiffness and damping of each flexible joint of a serial robot [14], while Bauchau and Nemani proposed some visco-elastic models suitable for elastic joint manipulators [15].

There are several varieties of elastic joint manipulators, e.g. robots with harmonic drives [16], cycloidal gears [17], and cable-driven actuation [18]. In the case of cable-driven manipulators, joints elasticity is introduced by a set of cables that transfer the motion from the actuators to the joints. Typically, a cable-driven manipulator is composed of a robotic arm and an actuation system, which includes actuators and cables. This structure allows separating the actuators from the robotic arm, typically placing them in a chassis at the base of the manipulator, reducing the size and weight of the robotic arm and increasing its payload capabilities. Moreover, it keeps the actuators outside the workspace, which could be an important advantage if the robot is designed to operate in harsh environments. An example would be in industrial inspection tasks, where the environment is often dangerous and narrow. The small dimensions of the robotic arm and the protection of the actuators make cable-driven manipulators particularly suitable for such applications, especially if their ability to move inside confined environments is increased by hyper-redundancy. Several examples of hyper-redundant cable-driven manipulators are present in literature, like the continuum robot proposed by Dong et al. [19] and the long-reach cable-driven manipulator designed by Canali et al. [20]. For these reasons, cable-driven manipulators are widely employed in industrial environments to increase workers' safety and reduce plant downtime due to inspection tasks. According to SPARC, these are both priority objectives for industries [21].

One of the most critical aspects of cable-driven manipulators design is the material of cables themselves. Cables can be made of stainless steel [22], or synthetic fibre, as in the Super Dragon robot [23]. A comparison between the physical properties of these two materials was performed by Horigome and Endo in 2016 [24], who also conducted repetitive bending experiments on synthetic fibre cables in 2018 [25]. This work suggested that synthetic fibre cables have many advantages with respect to steel cables: (i) they are lighter, which further reduces the robotic arm weight, (ii) they can wrap around pulleys with smaller diameter, which allows reducing robotic arm dimensions, and (iii) they have a higher tensile strength.

As already mentioned, to obtain an accurate dynamic model of an elastic joint manipulator, which is crucial to perform model-based control, the joints flexibility must be considered in the robot model. In the case of cable-driven manipulators, this consists of modelling the robotic arm and the dynamic behaviour of the cables. Regarding the robotic arm, the Lagrange formulation is the basis of the first works on manipulator modelling [26,27]. Orin et al. presented a recursive Newton–Euler method to analyse the dynamics of spatial open-chain mechanisms [28], while Hollerbach developed an efficient algorithm to derive Lagrange equations of a serial manipulator [29]. In 1982, Silver demonstrated the equivalence of the Lagrange and Newton–Euler methods [30]. The most relevant Newton–Euler algorithms are the Composite Rigid Body Algorithm [31] and the Articulated Body Algorithm [32]. Finally, Featherstone presented a comparison between recursive Newton–Euler algorithms [33]. Over the years, many methods to add the cables dynamics to the model of the manipulator have been introduced. Zhao et al. proposed a complete model of a cable-driven manipulator derived using the Lagrangian dynamics [34]. Fichera and Grossard proposed a framework to produce a piece-wise elastic torque model for cable-driven robots exploiting standard procedures to identify the parameters [35], while Choi and Park described the main characteristics of cables through an integrated elasto-plastic model [36]. In 2018, Takata et al. modelled synthetic fibre cables with Flory's model and demonstrated that, by applying a sufficient preload, it can be reduced to a four elements model [37].

Cable-driven manipulators are non-linear systems. The literature presents many studies related to the control of elastic joint manipulators motion using non-linear control strategies. For a traditional PD controller, the robustness to uncertainties on mass matrix parameters and friction model was proved for elastic joint robots by Tomei in 1991 [38]. Albu-Schäffer et al. exploited the passivity properties of cable-driven manipulators to produce a passivity-based control framework for elastic joint manipulators [39]. A passivity-based control strategy was also proposed in 2014 by Caverly and Forbes for a planar cable-driven manipulator [40]. In 2013, Wang et al. developed a visual servo control for a soft cable-driven manipulator, whose mechanical compliance and number of Degrees of Freedom (DoFs) make it particularly suitable for operating in confined environments [41] . In the same year, Salimi et al. proposed a gain scheduling controller for a cable-driven robotic system [42], while, in 2018, Wang et al. studied an adaptive time-delay control scheme composed of a time delay estimation, injected dynamics, and adaptive law [43]. Endo et al. proposed a global feedback linearisation that stabilises the system using static state feedback, which requires full-state feedback up to the third derivative of the joints position [23]. An adaptive fractional-order nonsingular terminal sliding mode control was applied to a 2 DoFs manipulator by Wang et al. in 2019 and 2020 [44,45]. In 2021, Sun et al. proposed a Fuzzy-PID controller for cable-driven parallel robots, which was tested on several different kinds of robots and whose performance was compared with an active control method and a passive control scheme [46].

In literature, a common practice is using a simplified model of synthetic fibre cables to design model-based controllers for cable-driven manipulators. The most common approach is modelling synthetic fibre cables as linear springs. Many studies have demonstrated the Lyapunov stability of cable-driven manipulators regulated by controllers based on these simplified models [46]. Conversely, although modelling the behaviour of cables has been deeply investigated and has reached remarkable results in terms of accuracy, the literature presents a considerable dearth of control strategies based on these more accurate models. Compared to previous studies, the key novelty of this work is the mathematical proof of closed-loop stability in the sense of Lyapunov for cable-driven manipulators regulated by a non-linear full-state feedback controller designed using the four elements model, which accurately describes the visco-elastic behaviour of synthetic fibre cables. This mathematical proof leads to some constraints on the matrices of the non-linear full-state feedback controller. At the time of this writing, the literature does not include any research approaching the problem using this model. Ultimately, this work aims to fill the research gap between the advanced modelling techniques of cables' dynamics and their application in model-based controller designs, introducing as the main contribution the mathematical proof of the Lyapunov stability for cable-driven manipulators described by one of these advanced modelling techniques and regulated by a model-based controller.

The proposed controller can stabilise cable-driven manipulators that respect the following design requirements: cables must be made of synthetic fibre and routed along the robotic arm in such a way that the linear motion of the cable is directly proportional to the angular motion of the joint.

The cable-driven manipulator presented by Ludovico et al. [47] is used in a simulated scenario to highlight the stable behaviour of the robotic system regulated by the proposed controller.

The results of this study represent an important starting point for improving the accuracy and precision of different model-based controllers for cable-driven manipulators, which is the main driver and motivation of this research study.

The paper is organised as follows. Section 2 describes the methods used to achieve the desired results, such as the mathematical tools and definitions, the dynamic model of the generic cable-driven manipulator, and the setup of a Simulink® simulation. Section 3 includes the proof of the stability of the closed-loop system. Section 4 reports and discuss the results of the mathematical proof described in the previous section and the results of the simulation. In Section 5, finally, a brief conclusion is given.

2. Material and methods

This section contains a brief explanation of the mathematical tools used in the paper, an overview of the robotic structure, the formalisation of the dynamic model of the complete system, the description of the control strategy applied to the system, and a summary of the stability theory used to verify that the chosen regulation scheme stabilises the system. Finally, the implementation of a Simulink® simulation is described.

2.1. Mathematical tools

Given a scalar $a \in \mathbb{R}$,

$$A = \operatorname{diag}(a)_n \in \mathbb{R}^{n\times n}$$

is the diagonal matrix with all entries equal to a. Likewise, given a set of scalars $\{b_i \in \mathbb{R} : i = 1, \dots, n\}$,

$$B = \operatorname{diag}(b_i)_n \in \mathbb{R}^{n\times n}$$

is the diagonal matrix whose main diagonal is composed of the scalars $\{b_i \in \mathbb{R} : i = 1, \dots, n\}$.

Given a square invertible matrix $S \in \mathbb{R}^{n\times n}$,

$$S^{-T} = \left(S^T\right)^{-1}.$$

Given a square matrix $Z \in \mathbb{R}^{n\times n}$, its symmetric part is defined as:

$$Z_s = \frac{1}{2}\left(Z + Z^T\right).$$

Given a vector $\boldsymbol{v} \in \mathbb{R}^{n\times 1}$, whose components are defined as $v_i \in \mathbb{R}$, its Euclidean Norm is defined as:

$$\|\boldsymbol{v}\|_2 = \sqrt{\sum_{i=1}^{n} v_i^2}.$$

Given a symmetric matrix $O \in \mathbb{R}^{n\times n}$, its Spectral Norm is defined as follows:

$$\|O\| = \sqrt{\lambda_{max}\left(O^T O\right)} = |\lambda_{max}(O)|,$$

where $\lambda_{max}(O)$ denotes the maximum eigenvalue of O. In a similar way, $\lambda_{min}(O)$ denotes the minimum eigenvalue of O.

A matrix $Q \in \mathbb{R}^{n\times n}$ is called positive definite, whose notation is $Q \succ 0$, if

$$\langle \boldsymbol{v}, Q\boldsymbol{v}\rangle = \boldsymbol{v}^T Q \boldsymbol{v} > 0\,,\ \forall \boldsymbol{v} \neq \boldsymbol{0},$$

while it is called positive semi-definite, whose notation is $Q \succeq 0$, if

$$\langle \boldsymbol{v}, Q\boldsymbol{v}\rangle = \boldsymbol{v}^T Q \boldsymbol{v} \geq 0\,,\ \forall \boldsymbol{v}.$$

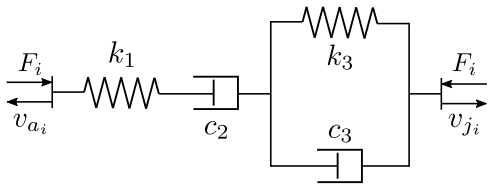

Fig. 1. Four elements model.

According to Johnson [48], a square matrix $Q \in \mathbb{R}^{n\times n}$ is positive (semi-)definite if and only if its symmetric part Q_s is positive (semi-)definite.

$$\begin{cases} Q \succ 0 \iff Q_s \succ 0 \\ Q \succeq 0 \iff Q_s \succeq 0 \end{cases}.$$

A square matrix $Q \in \mathbb{R}^{n\times n}$ is negative (semi-)definite, whose notation is $Q \prec 0$ ($Q \preceq 0$), if and only if $-Q$ is positive (semi-)definite:

$$\begin{cases} Q \prec 0 \iff -Q \succ 0 \\ Q \preceq 0 \iff -Q \succeq 0 \end{cases}.$$

If $Q = Q^T$, Q is positive (negative) definite if all its eigenvalues are positive (negative); if the eigenvalues are greater (less) or equal to zero, Q is positive (negative) semi-definite.

2.2. Robotic structure

A generic cable-driven manipulator is usually divided into two main parts: the robotic arm and the actuation system, composed of cables and actuators. Regarding the former, in this paper, a cable-driven manipulator with a rigid robotic arm composed of n revolute joints is considered. About the latter part, the actuation system is assumed to be composed of two synthetic fibre cables per joint, routed along the robotic arm so that the map between the linear velocity of the cables and the angular velocity of the joints is constant and decoupled. In literature, many examples of cable-driven manipulators that respect these assumptions can be found, like the one designed by Canali et al. [20].

2.3. Dynamic model

In this section, the dynamic model of the complete system is extrapolated and described. First, the dynamic model of cables is investigated, then the dynamics of the rigid robotic arm is reported, and finally the overall dynamic model introduced by Ludovico [49] is summarised.

2.3.1. Dynamic model of cables

In many works, cables of cable-driven manipulators are modelled as linear springs. In this work, instead, cables are modelled using the four elements model, which includes the visco-elastic phenomena.

The four elements model, shown in Fig. 1, is a series of (i) a spring element k_1, which describes the elasticity, (ii) a damper element c_2, which is related to viscosity, and (iii) a parallel of a spring k_3 and a damper c_3, which models the retarded elasticity.

In the case of a manipulator that satisfies the assumptions described in Section 2.2, each joint is driven by two cables, one pulled in the opposite direction with respect to the other during the robot motion. In this context, thus, the ith couple of cables

driving the ith joint can be modelled as follows:

$$\begin{cases} \dot{s}_{11_i} = -k_1 d_1 s_{11_i} + k_3 d_2 s_{21_i} + \dfrac{v_{j_i} - v_{a_i}}{l_i} \\ \dot{s}_{21_i} = k_1 d_2 s_{11_i} - k_3 d_2 s_{21_i} \\ \dot{s}_{12_i} = -k_1 d_1 s_{12_i} + k_3 d_2 s_{22_i} - \dfrac{v_{j_i} - v_{a_i}}{l_i} \\ \dot{s}_{22_i} = k_1 d_2 s_{12_i} - k_3 d_2 s_{22_i} \\ \Delta F_i = k_1 \left(s_{11_i} - s_{12_i} \right) \end{cases} \tag{1}$$

where ΔF_i is the net force applied by the ith couple of cables, l_i is the length of the each cable composing the ith couple when no loads are applied, v_{j_i} and v_{a_i} are the linear velocity of the ith joint and of the ith cable, respectively, d_1 and d_2 are defined as

$$d_1 = \frac{c_2 + c_3}{c_2 c_3},$$
$$d_2 = \frac{1}{c_3},$$

and s_{11_i}, s_{21_i}, s_{12_i}, and s_{22_i} represent the dimensionless strain of the ith couple of cables, defined such that

$$s_{11_i} + s_{21_i} = \frac{l_{d_i} - l_i}{l_i},$$
$$s_{12_i} + s_{22_i} = -\frac{l_{d_i} - l_i}{l_i},$$

where l_{d_i} is the length of each cable of the ith couple when deformed by a load.

Defining a new set of variables as

$$\begin{bmatrix} \Delta s_{1_i} \\ \Delta s_{2_i} \end{bmatrix} = \begin{bmatrix} s_{11_i} - s_{12_i} \\ s_{21_i} - s_{22_i} \end{bmatrix}$$
$$\boldsymbol{\sigma}_1 = \begin{bmatrix} \Delta s_{1_1} & \cdots & \Delta s_{1_n} \end{bmatrix}^T,$$
$$\boldsymbol{\sigma}_2 = \begin{bmatrix} \Delta s_{2_1} & \cdots & \Delta s_{2_n} \end{bmatrix}^T,$$
$$\Delta \boldsymbol{F} = \begin{bmatrix} \Delta F_1 & \cdots & \Delta F_n \end{bmatrix}^T,$$

and exploiting (1), the dynamic model of the cables driving a cable-driven manipulator with n joints can be re-written as follows:

$$\begin{cases} \dot{\boldsymbol{\sigma}}_1 = -K_1 D_1 \boldsymbol{\sigma}_1 + K_3 D_2 \boldsymbol{\sigma}_2 + LR\dot{\boldsymbol{q}} - L\boldsymbol{u} \\ \dot{\boldsymbol{\sigma}}_2 = K_1 D_2 \boldsymbol{\sigma}_1 - K_3 D_2 \boldsymbol{\sigma}_2 \\ \Delta \boldsymbol{F} = K_1 \boldsymbol{\sigma}_1 \end{cases}, \tag{2}$$

where $\dot{\boldsymbol{q}}$ is the vector of angular velocities of the joints, $\boldsymbol{u}$ is the system input, i.e. the vector of linear velocities of the anchor points of cables, L is a diagonal matrix composed of the inverse of the lengths of the cables, R is the map between the linear motion of the cables and the angular motion of the joints, K_1 and K_3 are diagonal matrices representing the springs k_1 and k_3 for all the cables, and D_1 and D_2 are diagonal matrices including the viscosity for all the cables. Therefore, using the definitions given in Section 2.1:

$$L = \operatorname{diag}\left(\frac{2}{l_i}\right)_n \succ 0,\ i = 1, \ldots, n,$$
$$R = \operatorname{diag}\left(r_i\right)_n \succ 0,\ i = 1, \ldots, n,$$
$$K_1 = \operatorname{diag}\left(k_1\right)_n \succ 0,$$
$$K_3 = \operatorname{diag}\left(k_3\right)_n \succ 0,$$
$$D_1 = \operatorname{diag}\left(d_1\right)_n \succ 0,$$
$$D_2 = \operatorname{diag}\left(d_2\right)_n \succ 0.$$

2.3.2. Dynamic model of the robotic arm

The dynamic model of a rigid robotic arm can be derived from the Lagrange's equations

$$\frac{d}{dt}\frac{\partial \mathscr{L}}{\partial \dot{q}_i} - \frac{\partial \mathscr{L}}{\partial q_i} = \tau_i \quad i = 1, \ldots, n, \tag{3}$$

where the Lagrangian

$$\mathscr{L} = T - U$$

is expressed as the difference between the kinetic energy T and the potential energy U, while τ_i is the generalised force at ith joint and q_i and $\dot{q}_i$ are the ith joint position and velocity, respectively. Since the robotic arm is rigid, the potential energy U comprises only the gravitational contribution:

$$U = U_g.$$

The kinetic energy is a quadratic form of the joint velocities, i.e.

$$T = \frac{1}{2}\dot{\boldsymbol{q}}^T M(\boldsymbol{q})\dot{\boldsymbol{q}}, \tag{4}$$

where $M(\boldsymbol{q}) \in \mathbb{R}^{n \times n}$ is the inertia matrix of the robotic manipulator and is defined such that

$$M(\boldsymbol{q}) = M^T(\boldsymbol{q}) \succ 0.$$

Substituting (4) in (3) and calculating the derivatives, the equations of motion can be derived:

$$M(\boldsymbol{q})\ddot{\boldsymbol{q}} + C(\boldsymbol{q}, \dot{\boldsymbol{q}})\dot{\boldsymbol{q}} + \boldsymbol{g}(\boldsymbol{q}) = \boldsymbol{\tau}, \tag{5}$$

where $\boldsymbol{\tau} \in \mathbb{R}^{n \times 1}$ is the joints forces vector, $\boldsymbol{g}(\boldsymbol{q}) \in \mathbb{R}^{n \times 1}$ is the gravity forces vector, whose ith element is

$$g_i(\boldsymbol{q}) = \frac{\partial U_g}{\partial q_i}, \tag{6}$$

and $C(\boldsymbol{q}, \dot{\boldsymbol{q}})\dot{\boldsymbol{q}} \in \mathbb{R}^{n \times 1}$, defined as

$$C(\boldsymbol{q}, \dot{\boldsymbol{q}})\dot{\boldsymbol{q}} = \dot{M}(\boldsymbol{q})\dot{\boldsymbol{q}} - \frac{1}{2}\left[\frac{\partial}{\partial \boldsymbol{q}}\left(\dot{\boldsymbol{q}}^T M(\boldsymbol{q})\dot{\boldsymbol{q}}\right)\right]^T,$$

is the vector of Coriolis and centrifugal forces. It is possible to factorise the vector $C(\boldsymbol{q}, \dot{\boldsymbol{q}})\dot{\boldsymbol{q}}$ in many ways, depending on the elements of the matrix $C(\boldsymbol{q}, \dot{\boldsymbol{q}})$. A possible way is to use the Christoffel symbols of the first type [5], which ensure that

$$\left[\dot{M}(\boldsymbol{q}) - 2C(\boldsymbol{q}, \dot{\boldsymbol{q}})\right] = -\left[\dot{M}(\boldsymbol{q}) - 2C(\boldsymbol{q}, \dot{\boldsymbol{q}})\right]^T.$$

Since $\boldsymbol{g}(\boldsymbol{q})$ is composed of trigonometric functions, a constant $\alpha \in \mathbb{R}^+$ exists such that

$$\left\| \frac{\partial \boldsymbol{g}(\boldsymbol{q})}{\partial \boldsymbol{q}} \right\| \leq \alpha,\ \forall \boldsymbol{q}, \tag{7}$$

which, considering two generic configurations $\boldsymbol{q}_a$ and $\boldsymbol{q}_b$, implies that

$$\left\| \boldsymbol{g}\left(\boldsymbol{q}_a\right) - \boldsymbol{g}\left(\boldsymbol{q}_b\right) \right\|_2 \leq \alpha \left\| \boldsymbol{q}_a - \boldsymbol{q}_b \right\|_2,\ \forall \left(\boldsymbol{q}_a, \boldsymbol{q}_b\right). \tag{8}$$

In the case of a cable-driven manipulator that meets the requirements described in Section 2.2, the vector of joints forces $\boldsymbol{\tau}$ is proportional to the cables strain, and can be defined as:

$$\boldsymbol{\tau} = -R^T K_1 \boldsymbol{\sigma}_1. \tag{9}$$

Finally, in virtue of (9), (5) can be re-written as follows:

$$\ddot{\boldsymbol{q}} = M^{-1}(\boldsymbol{q})\left[-C(\boldsymbol{q}, \dot{\boldsymbol{q}})\dot{\boldsymbol{q}} - \boldsymbol{g}(\boldsymbol{q}) - R^T K_1 \boldsymbol{\sigma}_1\right]. \tag{10}$$

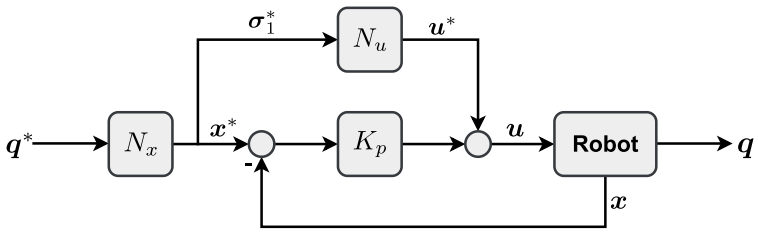

Fig. 2. Non-linear full-state feedback controller diagram.

2.3.3. Complete dynamic model

The complete dynamic model of the cable-driven manipulator is composed of the dynamic model of the cables, reported in (2), and the dynamic model of the rigid robotic arm, presented in (10). Thus, the dynamic model of the cable-driven manipulator is:

$$\begin{cases} \dot{\boldsymbol{\sigma}}_1 = -K_1 D_1 \boldsymbol{\sigma}_1 + K_3 D_2 \boldsymbol{\sigma}_2 + LR\dot{\boldsymbol{q}} - L\boldsymbol{u} \\ \dot{\boldsymbol{\sigma}}_2 = K_1 D_2 \boldsymbol{\sigma}_1 - K_3 D_2 \boldsymbol{\sigma}_2 \\ \ddot{\boldsymbol{q}} = M^{-1}(\boldsymbol{q})\left[-C(\boldsymbol{q},\dot{\boldsymbol{q}})\dot{\boldsymbol{q}} - \boldsymbol{g}(\boldsymbol{q}) - R^T K_1 \boldsymbol{\sigma}_1\right] \end{cases} . \tag{11}$$

The model reported in (11) ensures a higher precision than the simplified approaches mentioned in Section 1, since includes the visco-elastic behaviour of synthetic fibre cables.

2.4. Control strategy: full-state feedback control

This section is dedicated to the description of the full-state feedback controller used to stabilise the cable-driven manipulator modelled in (11).

Defining the state variable vector

$$\boldsymbol{x} = \begin{bmatrix} \boldsymbol{\sigma}_1^T & \boldsymbol{\sigma}_2^T & \boldsymbol{q}^T & \dot{\boldsymbol{q}}^T \end{bmatrix}^T ,$$

the dynamic model shown in (11) can be expressed in state-space representation

$$\begin{cases} \dot{\boldsymbol{x}} = f(\boldsymbol{x},\boldsymbol{u}) \\ \boldsymbol{y} = h(\boldsymbol{x}) \end{cases} , \tag{12}$$

where

$$f(\boldsymbol{x},\boldsymbol{u}) = \begin{bmatrix} -K_1 D_1 \boldsymbol{\sigma}_1 + K_3 D_2 \boldsymbol{\sigma}_2 + LR\dot{\boldsymbol{q}} - L\boldsymbol{u} \\ K_1 D_2 \boldsymbol{\sigma}_1 - K_3 D_2 \boldsymbol{\sigma}_2 \\ \dot{\boldsymbol{q}} \\ M^{-1}(\boldsymbol{q})\left[-C(\boldsymbol{q},\dot{\boldsymbol{q}})\dot{\boldsymbol{q}} - \boldsymbol{g}(\boldsymbol{q}) - R^T K_1 \boldsymbol{\sigma}_1\right] \end{bmatrix} , \tag{13}$$

$$h(\boldsymbol{x}) = \boldsymbol{q} .$$

To stabilise the non-linear system described in (12) and (13), a full-state feedback controller, whose schematic is shown in Fig. 2, is implemented. Besides the full-state feedback, the control input is enforced with an additional feed-forward signal, called $\boldsymbol{u}^*$, which, given the desired robot configuration $\boldsymbol{q}^*$, is computed as follows:

$$\boldsymbol{u}^* = L^{-1}\left[K_3 D_2 \boldsymbol{\sigma}_2^* - K_1 D_1 \boldsymbol{\sigma}_1^*\right] , \tag{14}$$

where $\boldsymbol{\sigma}_1^*$ and $\boldsymbol{\sigma}_2^*$ are the desired values of $\boldsymbol{\sigma}_1$ and $\boldsymbol{\sigma}_2$ and are evaluated by the N_x block, which computes the complete desired state vector $\boldsymbol{x}^*$ as follows:

$$\boldsymbol{x}^* = \begin{bmatrix} \boldsymbol{\sigma}_1^* \\ \boldsymbol{\sigma}_2^* \\ \boldsymbol{q}^* \\ \dot{\boldsymbol{q}}^* \end{bmatrix} = \begin{bmatrix} -K_1^{-1} R^{-T} \boldsymbol{g}\left(\boldsymbol{q}^*\right) \\ K_1 K_3^{-1} \boldsymbol{\sigma}_1^* \\ \boldsymbol{q}^* \\ \boldsymbol{0} \end{bmatrix} = N_x\left(\boldsymbol{q}^*\right) , \tag{15}$$

where $\boldsymbol{g}\left(\boldsymbol{q}^*\right)$ is the vector of gravity forces in the desired configuration, calculated on-line by the N_x block using the recursive Newton–Euler algorithm.

Given (15), $\boldsymbol{u}^*$ can be re-written in the more compact form

$$\boldsymbol{u}^* = N_u \boldsymbol{\sigma}_1^* ,$$

where

$$N_u = L^{-1} K_1 \left(D_1 + D_2\right) .$$

Applying the full-state feedback control strategy, thus, the control law is:

$$\boldsymbol{u} = K_p \boldsymbol{x}_e + \boldsymbol{u}^* , \tag{16}$$

where

$$\begin{aligned} &\boldsymbol{x}_e = \boldsymbol{x}^* - \boldsymbol{x} , \\ &K_p = \begin{bmatrix} K_{p_1} & K_{p_2} & K_{p_3} & K_{p_4} \end{bmatrix} , \end{aligned} \tag{17}$$

with

$$\left\{ K_{p_i} \in \mathbb{R}^{n \times n} : i = 1, \ldots, 4 \right\} .$$

Therefore, (16) can be re-written as

$$\begin{aligned} \boldsymbol{u} &= \begin{bmatrix} K_{p_1} & K_{p_2} & K_{p_3} & K_{p_4} \end{bmatrix} \begin{bmatrix} \boldsymbol{\sigma}_{e_1} \\ \boldsymbol{\sigma}_{e_2} \\ \boldsymbol{q}_e \\ \dot{\boldsymbol{q}}_e \end{bmatrix} + \boldsymbol{u}^* \\ &= K_{p_1} \boldsymbol{\sigma}_{e_1} + K_{p_2} \boldsymbol{\sigma}_{e_2} + K_{p_3} \boldsymbol{q}_e + K_{p_4} \dot{\boldsymbol{q}}_e + \boldsymbol{u}^* , \end{aligned} \tag{18}$$

where

$$\begin{aligned} \boldsymbol{\sigma}_{e_1} &= \boldsymbol{\sigma}_1^* - \boldsymbol{\sigma}_1 , \\ \boldsymbol{\sigma}_{e_2} &= \boldsymbol{\sigma}_2^* - \boldsymbol{\sigma}_2 , \\ \boldsymbol{q}_e &= \boldsymbol{q}^* - \boldsymbol{q} , \\ \dot{\boldsymbol{q}}_e &= \dot{\boldsymbol{q}}^* - \dot{\boldsymbol{q}} . \end{aligned} \tag{19}$$

2.5. Lyapunov stability theory

This section summarises the Lyapunov stability theory, which will be exploited in Section 3 to prove the stability of the closed-loop system.

Considering a generic non-linear system of the form shown in (12) and ($\boldsymbol{x} = \boldsymbol{x}^*$) as an equilibrium point of the system, if a scalar continuously differentiable function

$$V(\boldsymbol{x}) : \begin{cases} V(\boldsymbol{x}) = 0 , & \text{if } \boldsymbol{x} = \boldsymbol{x}^* \\ V(\boldsymbol{x}) > 0 , & \forall \boldsymbol{x} \neq \boldsymbol{x}^* \end{cases}$$

exists such that its time derivative along the system trajectory

$$\dot{V}(\boldsymbol{x}) = \frac{\partial V(\boldsymbol{x})}{\partial \boldsymbol{x}} \dot{\boldsymbol{x}} < 0 , \ \forall \boldsymbol{x} \neq \boldsymbol{x}^* ,$$

then the equilibrium point ($\boldsymbol{x} = \boldsymbol{x}^*$) of the non-linear system is asymptotically stable. If $\dot{V}(\boldsymbol{x}) \leq 0$, instead, the equilibrium point is stable. If $V(\boldsymbol{x})$ has the just described characteristics, it is a Lyapunov function for the system and the system is stable in the sense of Lyapunov.

2.6. Simulation

This section is dedicated to the Simulink® simulation performed to test the stability of the closed-loop system in a chosen case of study. For the simulation, the cable-driven manipulator

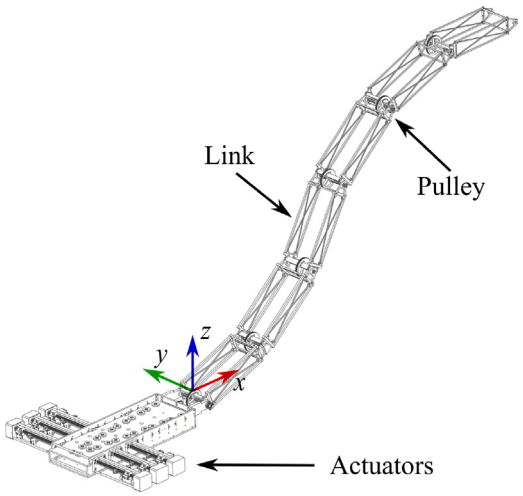

Fig. 3. CAD model of the cable-driven manipulator.
Source: Reprinted, with permission, from [47].
© 2021 IEEE.

Table 1
Zylon PBO cables four elements model parameters.

	Value	Uncertainty	Unit
K_1	2.933×10^5	1.73×10^4	N
c_2	5.78×10^9	1.33×10^9	N s
K_3	7.67×10^6	1.74×10^6	N
c_3	9.08×10^7	2.23×10^7	Ns

Table 2
Cable-driven hyper-redundant manipulator parameters.
Source: Reprinted, with permission, from [47].
© 2021 IEEE.

	J_1	J_2	J_3	J_4	J_5	J_6	Unit
m	2.16	2.16	1.55	1.55	1.3	1.3	kg
CoM	197	197	170	170	136	136	mm
l	500	500	500	500	500	500	mm
r	55	55	55	55	55	55	mm
l	1	1.5	2	2.5	2.9	3.4	m

presented by Ludovico et al. [47], which meets the requirements for being modelled as exposed in Section 2.3, is used. This section includes a description of the robotic platform and the simulation design.

2.6.1. Simulated robot

The cable-driven manipulator developed by Ludovico et al. [47] consists of six modules connected by six revolute joints, whose rotational axes are parallel one to the other, as shown in Fig. 3. This design constrains the manipulator motion on one plane. Each joint is composed of a circular pulley of radius r that is rigidly attached to its rigid link, which has length l: the couple composed of a link and its pulley forms one module.

Each module is driven by a synthetic fibre cable made of Zylon PBO, whose parameters of the four elements model are reported in Table 1. The cable is fixed on both sides to a linear actuator, is wrapped on the pulley, and transfers the motion of the actuator to the module through the friction with the pulley itself. Cables routing is realised through rolling bushings in such a way that cables pass along the neutral axis of each link, which generates a constant and decoupled map between the actuator linear velocity and joint angular velocity. This means that these two quantities are directly proportional one to the other.

Even if this robot has just one cable per joint, it is possible to consider the part of the cable passing below the pulley and the part passing above it as two different cables. Hence, it is possible to model the cable-driven manipulator shown in Fig. 3 with the model reported in Section 2.3.3, where the pulley radius r is the map between the linear motion of the cable and the angular motion of the joint. This means that, for this robot, matrix R is composed of the radius of the six pulleys. The geometric parameters of each joint J_i, are listed in Table 2, where m is the mass of each module and CoM is the location of its centre of mass.

2.6.2. Simulation design

The control strategy shown in Section 2.4 and depicted in Fig. 2 is applied to the robot described in Section 2.6.1 in a simulation implemented and executed in Simulink® to test the closed-loop system behaviour. In the simulation, the proportional gain K_p is chosen respecting the constraints extracted from the stability proof reported in Section 3. Since the system stability is proved for any closed-loop equilibrium point, the simulation is designed so that the regulated robot reaches different equilibrium points.

At the beginning of the simulation, the robot is set to a random initial configuration, whose relative equilibrium point is evaluated solving the static equation of the system dynamics. The initial value of the reference signal is the starting configuration, which is maintained for 30 s. Then, a sequence of nine steps is given as angular position reference to each joint of the robot. The amplitude of the steps is randomly generated in the interval $[-0.25, 0.25]$ rad, taking into account the joint limit of $[-\pi/3, \pi/3]$ rad. In this way, including the initial condition, the closed-loop system behaviour is tested at 10 equilibrium points. Since the state variable $\boldsymbol{\sigma}_2$ has a higher time constant with respect to the others, while the first eight intervals are 30 s long, the last two are 105 s long. In this way, as shown in Section 4, it is possible to appreciate the convergence of all the components of the state error, $\boldsymbol{x}_e$. With this reference signal design, which is depicted in Fig. 4, the simulation lasts 450 s.

3. Calculation: Lyapunov stability

In this section, the stability of the closed-loop system is proved exploiting the Lyapunov stability theory described in Section 2.5. All the mathematical definitions used in this section are summarised in Appendix.

Consider the following function as Lyapunov function candidate:

$$\begin{aligned} V(\boldsymbol{x}) &= \sum_{i=1}^{4} V_i(\boldsymbol{x}) \,, \\ V &:= V(\boldsymbol{x}) \,, \\ V_i &:= V_i(\boldsymbol{x}) \,, \end{aligned} \tag{20}$$

where

$$\begin{aligned} V_1 &= \frac{1}{2}\boldsymbol{e}^T G \boldsymbol{e} \,, \\ V_2 &= \frac{1}{2}\dot{\boldsymbol{q}}^T M \dot{\boldsymbol{q}} \,, \\ V_3 &= U_g(\boldsymbol{q}) - \boldsymbol{q}^T \boldsymbol{g}(\boldsymbol{q}^*) - U_g(\boldsymbol{q}^*) + \boldsymbol{q}^{*T} \boldsymbol{g}(\boldsymbol{q}^*) \,, \\ V_4 &= \frac{1}{2}\boldsymbol{q}_e^T G_2 \boldsymbol{q}_e \,, \end{aligned} \tag{21}$$

with

$$P = R^{-T} L^{-T} \succ 0 \,, \tag{22}$$

$$\boldsymbol{e} = P^T \boldsymbol{\sigma}_{e_1} - \boldsymbol{q}_e \,, \tag{23}$$

$$G = G^T \succ 0 \,, \tag{24}$$

$$G_2 = G_2^T \succ 0 : \lambda_{min}(G_2) > \alpha \,, \tag{25}$$

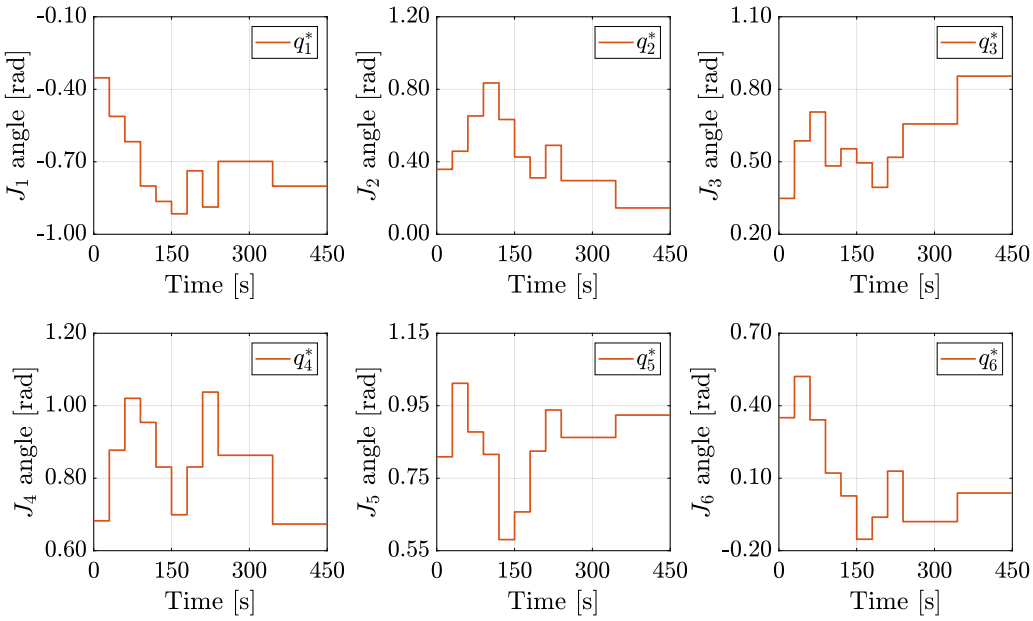

Fig. 4. Reference signal used in the simulation.

where $\lambda_{min}\,(G_2)$ represents the smallest eigenvalue of G_2.

Since V_1 and V_2 are quadratic forms, their positive-definiteness is ensured. Therefore, V is positive-definite if $V_3 + V_4$ is positive-definite. The stationary points of $V_3 + V_4$, which is function of $\boldsymbol{q}$, are given by the solutions of

$$\frac{\partial\,(V_3 + V_4)}{\partial \boldsymbol{q}} = \boldsymbol{g}(\boldsymbol{q}) - \boldsymbol{g}(\boldsymbol{q}^*) + G_2\boldsymbol{q}_e = 0\,, \tag{26}$$

which has the unique solution $\boldsymbol{q} = \boldsymbol{q}^*$. Moreover, in virtue of (7) and (25),

$$\frac{\partial^2\,(V_3 + V_4)}{\partial \boldsymbol{q}^2} = \frac{\partial \boldsymbol{g}(\boldsymbol{q})}{\partial \boldsymbol{q}} + G_2 > 0\,, \tag{27}$$

which means that $\boldsymbol{q} = \boldsymbol{q}^*$ is an absolute minimum for $V_3 + V_4$. Therefore, since

$$V_3 + V_4|_{\boldsymbol{q}=\boldsymbol{q}^*} = 0\,, \tag{28}$$

the constrain reported in (25) ensures the positive-definiteness of $V_3 + V_4$ and, consequently, of V.

The time derivative of (20) is

$$\dot{V} = \sum_{i=1}^{4} \dot{V}_i.$$

The verification of $\dot{V} \leq 0$, which is a sufficient condition for the stability in the sense of Lyapunov of the closed-loop system, is conducted considering each V_i function separately.

The time derivative of V_1 is

$$\dot{V}_1 = \boldsymbol{e}^T G P^T \dot{\boldsymbol{\sigma}}_{e_1} - \boldsymbol{e}^T G \dot{\boldsymbol{q}}_e,$$

which, using (2) and (19), becomes

$$\dot{V}_1 = -\,\boldsymbol{e}^T G P^T \left[-K_1 D_1 \boldsymbol{\sigma}_1 + K_3 D_2 \boldsymbol{\sigma}_2\right] + \boldsymbol{e}^T G P^T \left[L\boldsymbol{u} - LR\dot{\boldsymbol{q}} + L^T R^T \dot{\boldsymbol{q}}\right].$$

Exploiting the symmetry of L and R and (19), $\dot{V}_1$ can be re-written as follows:

$$\begin{aligned}\dot{V}_1 = &-\,\boldsymbol{e}^T G P^T \left[-K_1 D_1 (\boldsymbol{\sigma}_1^* - \boldsymbol{\sigma}_{e_1})\right] + \\ &-\,\boldsymbol{e}^T G P^T \left[K_3 D_2 (\boldsymbol{\sigma}_2^* - \boldsymbol{\sigma}_{e_2})\right] + \boldsymbol{e}^T G P^T L\boldsymbol{u}\,.\end{aligned} \tag{29}$$

Substituting (16) in (29), $\dot{V}_1$ can be re-written again as

$$\begin{aligned}\dot{V}_1 = &\ \boldsymbol{e}^T G P^T \left[\left(LK_{p_1} - K_1 D_1\right)\boldsymbol{\sigma}_{e_1} + LK_{p_3}\boldsymbol{q}_e + \right. \\ &+\ \left.\left(K_3 D_2 + LK_{p_2}\right)\boldsymbol{\sigma}_{e_2} + LK_{p_4}\dot{\boldsymbol{q}}_e\right] + \\ &+\ \boldsymbol{e}^T G P^T \left[L\boldsymbol{u}^* - K_1 D_1 \boldsymbol{\sigma}_1^* - K_3 D_2 \boldsymbol{\sigma}_2^*\right],\end{aligned}$$

which, in virtue of (14) and (19), reduces to:

$$\begin{aligned}\dot{V}_1 = &\ \boldsymbol{e}^T G P^T \left[\left(LK_{p_1} - K_1 D_1\right)\boldsymbol{\sigma}_{e_1} + LK_{p_3}\boldsymbol{q}_e\right] \\ &+\ \boldsymbol{e}^T G P^T \left[\left(K_3 D_2 + LK_{p_2}\right)\boldsymbol{\sigma}_{e_2} - LK_{p_4}\dot{\boldsymbol{q}}\right].\end{aligned}$$

Using (23), $\dot{V}_1$ can be re-written as follows:

$$\begin{aligned}\dot{V}_1 = &\ \begin{bmatrix}\boldsymbol{\sigma}_{e_1}^T & \boldsymbol{q}_e^T\end{bmatrix} H \begin{bmatrix}\boldsymbol{\sigma}_{e_1} \\ \boldsymbol{q}_e\end{bmatrix} + \boldsymbol{\sigma}_{e_1}^T P G P^T \left(K_3 D_2 + LK_{p_2}\right)\boldsymbol{\sigma}_{e_2} + \\ &-\,\boldsymbol{q}_e^T G P^T \left(K_3 D_2 + LK_{p_2}\right)\boldsymbol{\sigma}_{e_2} + \boldsymbol{q}_e^T G P^T LK_{p_4}\dot{\boldsymbol{q}} - \boldsymbol{\sigma}_{e_1}^T P G P^T LK_{p_4}\dot{\boldsymbol{q}}\,,\end{aligned} \tag{30}$$

where

$$H = \begin{bmatrix}PH_1 & PH_2 \\ -H_1 & -H_2\end{bmatrix},$$

$$H_1 = GP^T\left(LK_{p_1} - K_1 D_1\right),$$

$$H_2 = GP^T LK_{p_3}\,.$$

Setting

$$K_{p_2} = -L^{-1} K_3 D_2$$

and using (22), (30) reduces to:

$$\dot{V}_1 = \begin{bmatrix}\boldsymbol{\sigma}_{e_1}^T & \boldsymbol{q}_e^T\end{bmatrix} H \begin{bmatrix}\boldsymbol{\sigma}_{e_1} \\ \boldsymbol{q}_e\end{bmatrix} - \boldsymbol{e}^T G R^{-T} K_{p_4}\dot{\boldsymbol{q}}\,. \tag{31}$$

The time derivative of V_2 is

$$\dot{V}_2 = \dot{\boldsymbol{q}}^T M\ddot{\boldsymbol{q}} + \frac{1}{2}\dot{\boldsymbol{q}}^T \dot{M}\dot{\boldsymbol{q}},$$

which, in virtue of (10), becomes

$$\dot{V}_2 = \dot{\boldsymbol{q}}^T \left[-C(\boldsymbol{q},\dot{\boldsymbol{q}})\dot{\boldsymbol{q}} + \frac{1}{2}\dot{M}\dot{\boldsymbol{q}} - \boldsymbol{g}(\boldsymbol{q}) - R^T K_1 \boldsymbol{\sigma}_1\right]. \tag{32}$$

Since $\left[\dot{M}(\boldsymbol{q}) - 2C(\boldsymbol{q},\dot{\boldsymbol{q}})\right]$ is skew-symmetric,

$$\dot{\boldsymbol{q}}^T \left[\dot{M}(\boldsymbol{q}) - 2C(\boldsymbol{q},\dot{\boldsymbol{q}})\right]\dot{\boldsymbol{q}} = 0$$

and, therefore, (32) reduces to:

$$\dot{V}_2 = -\dot{\boldsymbol{q}}^T \boldsymbol{g}(\boldsymbol{q}) - \dot{\boldsymbol{q}}^T R^T K_1 \boldsymbol{\sigma}_1 \,. \tag{33}$$

The time derivative of V_3 is

$$\dot{V}_3 = \frac{\partial U_g(\boldsymbol{q})}{\partial \boldsymbol{q}} \dot{\boldsymbol{q}} - \dot{\boldsymbol{q}}^T \boldsymbol{g}(\boldsymbol{q}^*),$$

which, exploiting (6), can be re-written as

$$\dot{V}_3 = \boldsymbol{g}(\boldsymbol{q})^T \dot{\boldsymbol{q}} - \dot{\boldsymbol{q}}^T \boldsymbol{g}(\boldsymbol{q}^*),$$

which, in virtue of (15), can be re-written again in the form

$$\dot{V}_3 = \boldsymbol{g}(\boldsymbol{q})^T \dot{\boldsymbol{q}} + \dot{\boldsymbol{q}}^T R^T K_1 \boldsymbol{\sigma}_1^* \,. \tag{34}$$

The combination of (33) and (34) implies that

$$\dot{V}_2 + \dot{V}_3 = \dot{\boldsymbol{q}}^T R^T K_1 \boldsymbol{\sigma}_{e_1} \,. \tag{35}$$

The time derivative of V_4 is

$$\dot{V}_4 = \boldsymbol{q}_e^T G_2 \dot{\boldsymbol{q}}_e,$$

which, using (19), becomes

$$\dot{V}_4 = -\boldsymbol{q}_e^T G_2 \dot{\boldsymbol{q}} \,. \tag{36}$$

Given (31), (35), and (36), the time derivative of the Lyapunov function proposed in (20), reduces to:

$$\begin{aligned} \dot{V} = \; & \dot{V}_1 + \dot{V}_2 + \dot{V}_3 + \dot{V}_4 = \\ = \; & \begin{bmatrix} \boldsymbol{\sigma}_{e_1}^T & \boldsymbol{q}_e^T \end{bmatrix} H \begin{bmatrix} \boldsymbol{\sigma}_{e_1} \\ \boldsymbol{q}_e \end{bmatrix} - \boldsymbol{\sigma}_{e_1}^T P G R^{-T} K_{p_4} \dot{\boldsymbol{q}} \\ & + \boldsymbol{q}_e^T G R^{-T} K_{p_4} \dot{\boldsymbol{q}} + \dot{\boldsymbol{q}}^T R^T K_1 \boldsymbol{\sigma}_{e_1} - \boldsymbol{q}_e^T G_2 \dot{\boldsymbol{q}} \,. \end{aligned} \tag{37}$$

Choosing G, G_2, and K_{p_4} as follows:

$$\begin{aligned} & G = P^{-1} K_1^T R K_{p_4}^{-1} R^T \succ 0 \,, \\ & G_2 = G R^{-T} K_{p_4} = P^{-1} K_1^T R \succ 0 \,, \\ & K_{p_4} = \operatorname{diag}\left(k_{p_{4_i}}\right)_n \,, \; \left\{ k_{p_{4_i}} \in \mathbb{R}^+ : i = 1, \ldots, n \right\}, \end{aligned}$$

G and G_2 are both diagonal, and thus symmetric, as required by (24) and (25). Therefore, (37) reduces to:

$$\dot{V} = \begin{bmatrix} \boldsymbol{\sigma}_{e_1}^T & \boldsymbol{q}_e^T \end{bmatrix} H \begin{bmatrix} \boldsymbol{\sigma}_{e_1} \\ \boldsymbol{q}_e \end{bmatrix} \,, \tag{38}$$

which is a quadratic form that is less or equal to zero for any $(\boldsymbol{\sigma}_{e_1}, \boldsymbol{q}_e)$ if H is negative semi-definite. In sight of (38), then, the closed-loop system is stable if

$$H \preceq 0 \iff H_s \preceq 0 \implies \dot{V} \leq 0,$$

where H_s is the symmetric part of H and is defined as

$$H_s = \begin{bmatrix} P H_1 & \frac{1}{2}\left(P H_2 - H_1\right) \\ \frac{1}{2}\left(P H_2 - H_1\right) & -H_2 \end{bmatrix} . \tag{39}$$

The matrix H_s, and consequently H, is negative semi-definite if and only if, considering two generic vectors $\boldsymbol{v} \in \mathbb{R}^{n\times 1}$ and $\boldsymbol{w} \in \mathbb{R}^{n\times 1}$, the following statement holds:

$$\begin{aligned} & \boldsymbol{z} = \begin{bmatrix} \boldsymbol{v}^T & \boldsymbol{w}^T \end{bmatrix}^T \,, \\ & \boldsymbol{z}^T H_s \boldsymbol{z} \leq 0 \,, \forall \boldsymbol{z} \neq \boldsymbol{0} \,, \end{aligned}$$

which, using (39), becomes:

$$\begin{aligned} \boldsymbol{z}^T H_s \boldsymbol{z} = \; & \boldsymbol{v}^T P H_1 \boldsymbol{v} + \frac{1}{2} \boldsymbol{v}^T \left(P H_2 - H_1\right) \boldsymbol{w} \\ & + \frac{1}{2} \boldsymbol{w}^T \left(P H_2 - H_1\right) \boldsymbol{v} - \boldsymbol{w}^T H_2 \boldsymbol{w} \leq 0 \,. \end{aligned} \tag{40}$$

Assuming all K_{p_i} as diagonal matrices, i.e.

$$K_{p_i} = \operatorname{diag}\left(k_{p_{i_j}}\right)_n \,, \tag{41}$$

where

$$\left\{ k_{p_{i_j}} \in \mathbb{R} : \; i = 1, \ldots, 4 \,, \; j = 1, \ldots, n \right\},$$

both the matrices H_1 and H_2 are diagonal as well. Thus, re-defining H_1, H_2, and P as follows:

$$\begin{aligned} & H_1 = \operatorname{diag}\left(h_{1_i}\right)_n \,, \left\{ h_{1_i} \in \mathbb{R} : i = 1, \ldots, n \right\} \,, \\ & H_2 = \operatorname{diag}\left(h_{2_i}\right)_n \,, \left\{ h_{2_i} \in \mathbb{R} : i = 1, \ldots, n \right\} \,, \\ & P = \operatorname{diag}\left(p_i\right)_n \,, \left\{ p_i \in \mathbb{R} : i = 1, \ldots, n \right\} \,, \end{aligned} \tag{42}$$

condition (41) allows to reduce (40) to:

$$\boldsymbol{v}^T P H_1 \boldsymbol{v} + \boldsymbol{v}^T (P H_2 - H_1) \boldsymbol{w} - \boldsymbol{w}^T H_2 \boldsymbol{w} \leq 0,$$

which, choosing

$$H_1 = -P H_2,$$

can be further simplified as

$$-\boldsymbol{v}^T P^2 H_2 \boldsymbol{v} + 2 \boldsymbol{v}^T P H_2 \boldsymbol{w} - \boldsymbol{w}^T H_2 \boldsymbol{w} \leq 0 \,. \tag{43}$$

Given (42) and assuming v_i and w_i as the ith components of $\boldsymbol{v}$ and $\boldsymbol{w}$, respectively, (43) can be re-written as follows:

$$\sum_{i=1}^{n} \left(p_i^2 h_{2_i} v_i^2 - 2 p_i h_{2_i} v_i w_i + h_{2_i} w_i^2 \right) \geq 0,$$

which can be re-written again in the form:

$$\sum_{i=1}^{n} \left[h_{2_i} \left(p_i v_i - w_i \right)^2 \right] \geq 0 \,. \tag{44}$$

Setting

$$\left\{ h_{2_i} > 0 : i = 1, \ldots, n \right\} \implies H_2 \succ 0,$$

inequality (44) is verified $\forall(\boldsymbol{v}, \boldsymbol{w})$, since each element of the summation is non negative. Thus, $H_s \preceq 0$ if

$$\begin{cases} H_2 \succ 0 \\ H_1 = -P H_2 \end{cases} , \tag{45}$$

which implies that $\dot{V} \leq 0$. Consequently, V is a Lyapunov function for the closed-loop system and, therefore, the equilibrium point $(\boldsymbol{x} = \boldsymbol{x}^*)$ of the closed-loop system is stable.

Constraints reported in (45) can be translated in the following constraints on K_{p_1} and K_{p_3}:

$$\begin{cases} K_{p_1} = L^{-1} K_1 D_1 - P K_{p_3} \\ K_{p_3} \succ 0 \end{cases} .$$

To summarise, if all K_{p_i} are diagonal matrices such that

$$\begin{aligned} & K_{p_1} = L^{-1} K_1 D_1 - P K_{p_3} \,, \\ & K_{p_2} = -L^{-1} K_3 D_2 \,, \\ & K_{p_3} \succ 0 \,, \\ & K_{p_4} \succ 0 \,, \end{aligned} \tag{46}$$

and if G_2 respects condition (25), then the equilibrium point $(\boldsymbol{x} = \boldsymbol{x}^*)$ of the closed-loop system described in (11), (14), and (16) is stable and the system is stable in the sense of Lyapunov.

4. Results and discussion

This section exposes and discusses the results obtained by the mathematical calculation that proved the closed-loop stability and the results of the simulation described in Section 2.6.

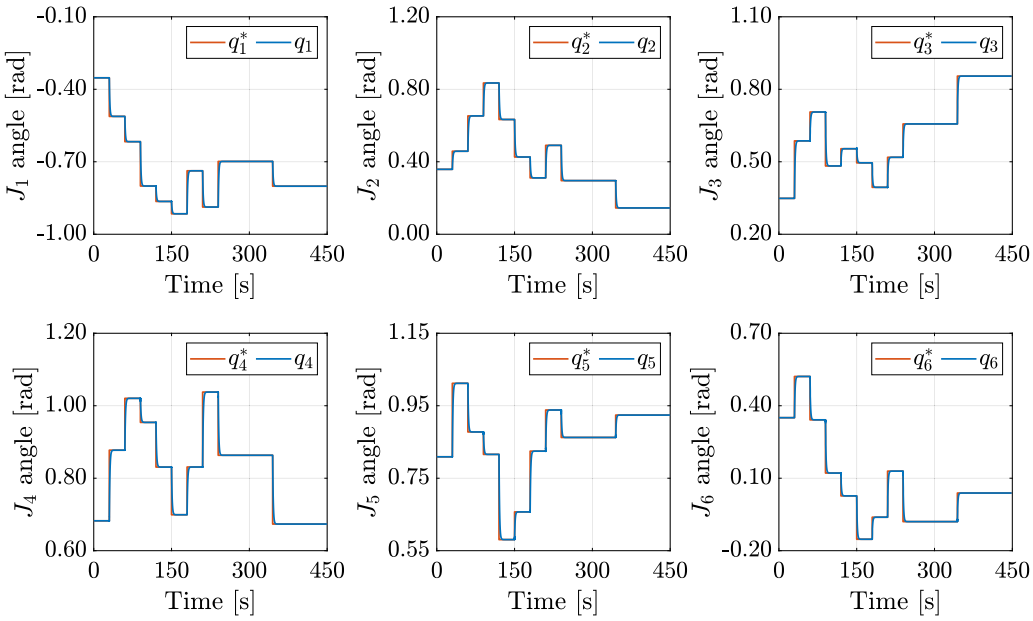

Fig. 5. Response of the closed-loop system in the simulation.

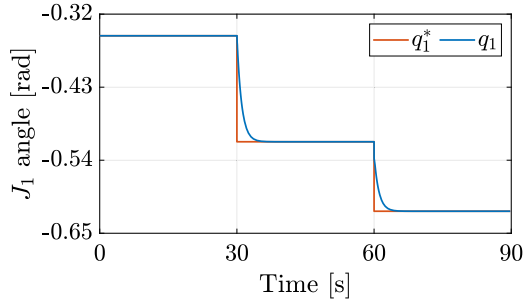

Fig. 6. Response of the first joint in the interval [0, 90] s to highlight the transient in the first two steps.

4.1. Stability results

The calculation provided in Section 3 demonstrates that the robotic structure modelled in (11) can be stabilised in the sense of Lyapunov by the non-linear full-state feedback controller illustrated in Section 2.4. This result can be achieved by choosing the elements $K_{p_i} \in \mathbb{R}^{n\times n}$ of the gain $K_p \in \mathbb{R}^{n\times 4n}$, defined in (17), as diagonal matrices where n is the number of joints of the manipulator. According to (46), matrices K_{p_1} and K_{p_2} have a specific form, which depends on K_{p_3} for the former and is constant for the latter, while K_{p_3} and K_{p_4} need to be positive definite. Therefore, the desired performance of the closed-loop system depends only on the tuning of the gains K_{p_3} and K_{p_4}, which control the joints angular position and velocity, respectively. Since both K_{p_3} and K_{p_4} are diagonal, the tuning problem consists in tuning the $2n$ entries of the two matrices.

Given (46), the closed-loop system is stable even if K_{p_1} is a matrix of zeros, condition that occurs when

$$K_{p_3} = P^{-1}L^{-1}K_1D_1.$$

This particular case implies that the strain $\boldsymbol{\sigma}_1$ is not used as feedback signal, leading to a degradation of the closed-loop system performance.

Lyapunov stability theory ensures that the set of conditions reported in (46) stabilises the equilibrium point of the closed-loop system, but it does not assert that it is the only combination of K_{p_i} that achieve this goal. Indeed, the choice of a different Lyapunov function or a change of the assumptions on K_p could lead to other solutions. For example, if K_{p_i} matrices were not forced to be diagonal, the reduction of (40) to the square of a binomial shown in (44) would not be possible, forcing matrices H_1 and H_2 to satisfy different conditions. An alternative condition could be to choose K_{p_i} matrices such that $(PH_2 - H_1)$ is skew-symmetric and H_1 and H_2 are negative-definite and positive-definite, respectively. This solution leads to the stability of the closed-loop system but complicates the construction and tuning of a proper gain K_p, which must have a form simultaneously implying that $(PH_2 - H_1)$ is skew-symmetric, H_1 is negative-definite, and H_2 is positive-definite. Conversely, the constraint on K_{p_i} that forces them to be diagonal matrices still stabilises the system, gives them a simple structure and simplifies the procedure of tuning the proportional gain K_p to the choice of $2n$ values, which is a remarkable advantage of the solution presented in Section 3.

4.2. Simulation results

In sight of conditions (46), the simulation described in Section 2.6 is performed setting

$$K_{p_3} = K_{p_4} = I,$$

where $I \in \mathbb{R}^{n\times n}$ is the identity matrix. Fig. 6 shows the joints' angular position $\boldsymbol{q}$ response to the reference signal described in Section 2.6, while Fig. 5 highlights the first joint response transient during the first 90 s of the simulation, corresponding to the initial configuration and the first two steps of the reference signal. The behaviour of the state error vector $\boldsymbol{x}_e$ for the first joint during the whole simulation is reported in Fig. 7, which clearly shows its boundedness, as expected from a stable system controlled by a full-state feedback regulator. As already mentioned in Section 2.6.2, the time constant of $\boldsymbol{\sigma}_2$ is higher than the other states, therefore, its boundedness can be appreciated only in the last two steps of the reference signal, which have longer intervals. To better evaluate the behaviour of the simulated system, Fig. 8 shows the trend of three of the four components of the state error vector $\boldsymbol{x}_e$ for the first joint in a neighbourhood of the first step of the reference signal. This picture shows the stability of $\boldsymbol{\sigma}_{e_1}$, $\boldsymbol{q}_e$,

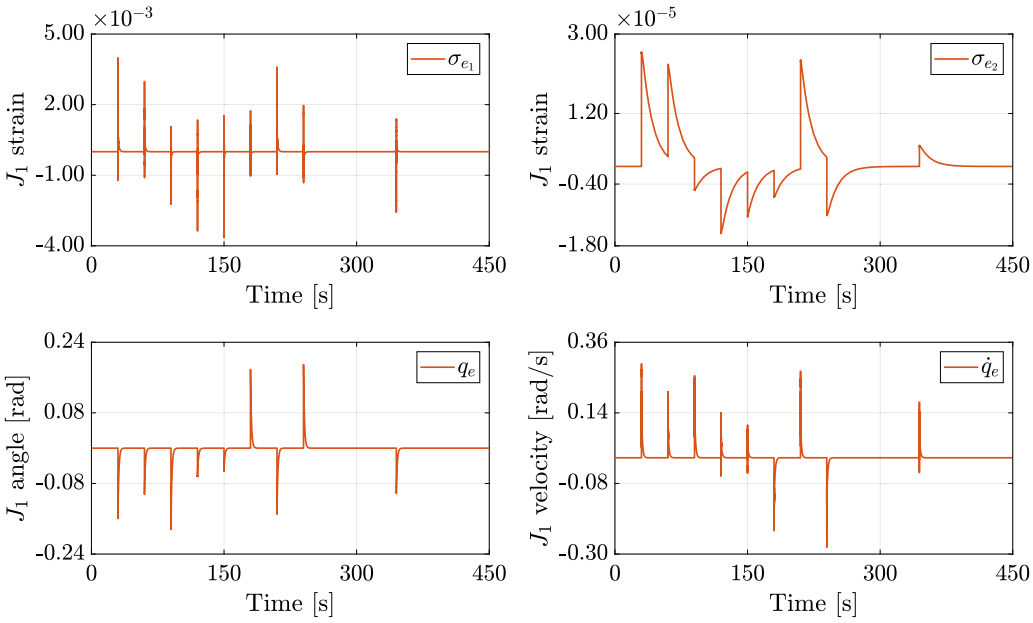

Fig. 7. State error $\boldsymbol{x}_e$ of the first joint in the simulation.

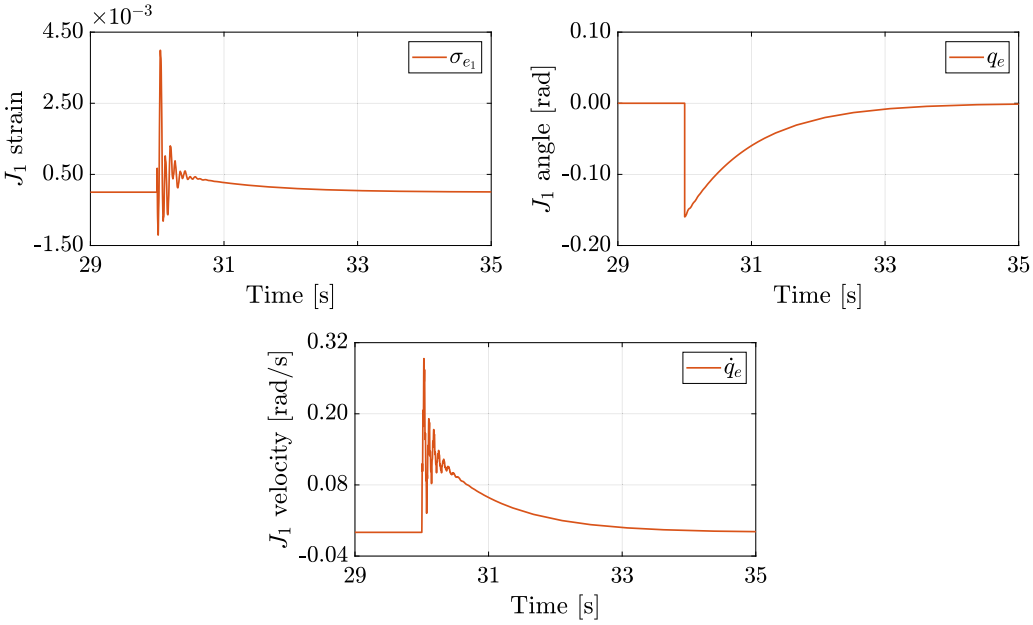

Fig. 8. Detail of $\boldsymbol{\sigma}_{e_1}$, $\boldsymbol{q}_e$, and $\dot{\boldsymbol{q}}_e$ variables of the first joint in the interval $[29, 35]$s to highlight the transient behaviour.

and $\dot{\boldsymbol{q}}_e$ at the selected equilibrium point, but it also highlights the oscillations of $\boldsymbol{\sigma}_{e_1}$ and $\dot{\boldsymbol{q}}_e$ during the transient. This chattering is mainly due to the discontinuity of the step reference signal and, in real applications, can be faced smoothing the reference signal and properly tuning the matrices K_{p_3} and K_{p_4}.

5. Conclusions

In this paper, the stability of a cable-driven manipulator controlled by a full-state feedback regulator is investigated. Assuming that the cable-driven manipulator has n revolute joints and two cables per joint routed along the structure so that the angular motion of the joint and the linear motion of the cable are proportional one to the other, a generic dynamic model of the robotic system is presented. The dynamics of the robotic arm is modelled using the Lagrangian formulation, while cables are modelled using the four elements model, which permits to include the linear visco-elastic phenomena. The application of this model, which is more accurate than the most commonly used spring model, is an unexplored territory and can be game-changing in the field of control of cable-driven manipulators.

A non-linear full-state feedback controller is designed for the just described robotic structure and the stability of the equilibrium point of the closed-loop system is demonstrated exploiting the direct method of Lyapunov. The stability study allows extrapolating some constraints for the proportional gain of the full-state feedback controller $K_p \in \mathbb{R}^{n\times 4n}$, which ensure the stability of the equilibrium point. A great advantage of the solution proposed in this work is the reduction of the problem of tuning the proportional gain K_p to the tuning of the two diagonal matrices $K_{p_3} \in \mathbb{R}^{n\times n}$ and $K_{p_4} \in \mathbb{R}^{n\times n}$, for a total of $2n$

values. Ultimately, this study presents a model-based controller for cable-driven manipulators whose main advantages are the use of a more accurate model compared to the ones in the literature and the simple tuning procedure, which consists of the choice of a few parameters. The Lyapunov stability proof of the closed-loop system is the main contribution of this study since the vast majority of the previous works provided stability proof using more simple models of cables' dynamics.

Finally, a Simulink® simulation is implemented and performed in such a way that the system reaches several random equilibrium points to test the proposed control strategy in a case study using the model of a pre-existing cable-driven manipulator. The simulation results confirms the stability of the selected closed-loop equilibrium points.

Although the proposed control strategy presents some restrictions on the design of the robot, which must satisfy the conditions stated in Section 2.2 and the constraint on G_2 reported in (25), and on the necessity of measuring or estimating all the state variables, this work represents a key starting point to develop model-based controllers for cable-driven manipulators actuated by synthetic fibre cables, modelled with the four elements model. The next step will be tuning the proportional gain to obtain the desired performance of the closed-loop system and comparing its behaviour with other control strategies found in the literature. The proposed approach strongly depends on the dynamic model of the system and, therefore, could be affected by parameters uncertainty. To reject these possible inaccuracies and potential external disturbances, the controller here presented could be modified to increase its robustness, such as considering sliding mode algorithms, integral action, or adaptive control techniques, like gain scheduling, fuzzy adaptive control, neural networks, or iterative learning algorithms. Finally, implementing the controller on a real robotic platform is a part of the future works that get inspiration from the study presented here.

Declaration of competing interest

The authors declare that they have no known competing financial interests or personal relationships that could have appeared to influence the work reported in this paper.

Appendix. Mathematical definitions and notations

This appendix summarises all the mathematical definitions and notations used in the paper. The mathematical tools exploited in the following are explained in Section 2.1.

$L = \text{diag}\left(\frac{2}{l_i}\right)_n \succ 0\,,\ i = 1, \dots, n$	where l_i is the i^{th} cable length
$R = \text{diag}\,(r_i)_n \succ 0\,,\ i = 1, \dots, n$	where r_i is the map between the i^{th} joint and the i^{th} cable motion
$K_1 = \text{diag}\,(k_1)_n \succ 0$	where k_1 is the first elastic constant of the four elements model
$K_3 = \text{diag}\,(k_3)_n \succ 0$	where k_3 is the second elastic constant of the four elements model
$D_1 = \text{diag}\,(d_1)_n \succ 0$	where d_1 is the first damping constant of the four elements model
$D_2 = \text{diag}\,(d_2)_n \succ 0$	where d_2 is the second damping constant of the four elements model
$\boldsymbol{\sigma}_1 \in \mathbb{R}^{n\times 1}$	the first cable strain vector
$\boldsymbol{\sigma}_2 \in \mathbb{R}^{n\times 1}$	the second cable strain vector
$\boldsymbol{q} \in \mathbb{R}^{n\times 1}$	robot configuration vector (joint angle)
$\dot{\boldsymbol{q}} \in \mathbb{R}^{n\times 1}$	robot joint velocity vector (joint angular velocity)
$\ddot{\boldsymbol{q}} \in \mathbb{R}^{n\times 1}$	robot joint acceleration vector (joint angular acceleration)
$\boldsymbol{x} = \left[\boldsymbol{\sigma}_1^T \quad \boldsymbol{\sigma}_2^T \quad \boldsymbol{q}^T \quad \dot{\boldsymbol{q}}^T\right]^T$	the state vector
$\boldsymbol{\sigma}_1^* \in \mathbb{R}^{n\times 1}$	the desired value of $\boldsymbol{\sigma}_1$
$\boldsymbol{\sigma}_2^* \in \mathbb{R}^{n\times 1}$	the desired value of $\boldsymbol{\sigma}_2$
$\boldsymbol{q}^* \in \mathbb{R}^{n\times 1}$	the desired value of $\boldsymbol{q}$
$\dot{\boldsymbol{q}}^* \in \mathbb{R}^{n\times 1}$	the desired value of $\dot{\boldsymbol{q}}$
$\boldsymbol{x}^* = \left[\boldsymbol{\sigma}_1^{*T} \quad \boldsymbol{\sigma}_2^{*T} \quad \boldsymbol{q}^{*T} \quad \dot{\boldsymbol{q}}^{*T}\right]^T$	the desired value of $\boldsymbol{x}$
$\boldsymbol{\sigma}_{e_1} = \boldsymbol{\sigma}_1^* - \boldsymbol{\sigma}_1$	the error on the first cable strain vector
$\boldsymbol{\sigma}_{e_2} = \boldsymbol{\sigma}_2^* - \boldsymbol{\sigma}_2$	the error on the second cable strain vector
$\boldsymbol{q}_e = \boldsymbol{q}^* - \boldsymbol{q}$	the error on the configuration vector (joint angle)
$\dot{\boldsymbol{q}}_e = \dot{\boldsymbol{q}}^* - \dot{\boldsymbol{q}}$	the error on the joint velocity vector (joint angular velocity)
$\boldsymbol{x}_e = \boldsymbol{x}^* - \boldsymbol{x}$	the state error vector
$\boldsymbol{u}^* = L^{-1}\left[K_3 D_2 \boldsymbol{\sigma}_2^* - K_1 D_1 \boldsymbol{\sigma}_1^*\right]$	the feed-forward signal included in the control input
$K_p = \left[K_{p_1} \quad K_{p_2} \quad K_{p_3} \quad K_{p_4}\right]$	the proportional gain of the full-state feedback controller
$K_{p_1} = \text{diag}\left(k_{p_{1_j}}\right)_n\,,\ j = 1, \dots, n$	the part of K_p controlling $\boldsymbol{\sigma}_1$
$K_{p_2} = \text{diag}\left(k_{p_{2_j}}\right)_n\,,\ j = 1, \dots, n$	the part of K_p controlling $\boldsymbol{\sigma}_2$
$K_{p_3} = \text{diag}\left(k_{p_{3_j}}\right)_n\,,\ j = 1, \dots, n$	the part of K_p controlling $\boldsymbol{q}$
$K_{p_4} = \text{diag}\left(k_{p_{4_j}}\right)_n\,,\ j = 1, \dots, n$	the part of K_p controlling $\dot{\boldsymbol{q}}$
$\boldsymbol{u} = K_p \boldsymbol{x}_e + \boldsymbol{u}^*$	the control input
$P = R^{-T} L^{-T} \succ 0$	a positive-definite diagonal matrix used in the Lyapunov function
$\boldsymbol{e} = P^T \boldsymbol{\sigma}_{e_1} - \boldsymbol{q}_e$	a vector used in the Lyapunov function
$G = G^T \succ 0$	a positive-definite symmetric matrix used in the Lyapunov function
$G_2 = G_2^T \succ 0$	a positive-definite symmetric matrix used in the Lyapunov function
$H = \begin{bmatrix} PH_1 & PH_2 \\ -H_1 & -H_2 \end{bmatrix}$	a matrix used in the Lyapunov function
$H_1 = GP^T\left(LK_{p_1} - K_1 D_1\right)$	a matrix included in H
$H_2 = GP^T LK_{p_3}$	a matrix included in H

References

[1] Robla-Gómez Sandra, Becerra Victor M, Llata José Ramón, Gonzalez-Sarabia Esther, Torre-Ferrero Carlos, Perez-Oria Juan. Working together: A review on safe human-robot collaboration in industrial environments. IEEE Access 2017;5:26754–73.

[2] Llale Josephine, Setati Matleko, Mavunda Success, Ndlovu Thando, Root David, Wembe Paulin. A review of the advantages and disadvantages of the use of automation and robotics in the construction industry. In: The construction industry in the fourth industrial revolution: proceedings of 11th construction industry development board (CIDB) postgraduate research conference, vol. 11. Springer; 2020, p. 197–204.

[3] Taylor Russell H. A perspective on medical robotics. Proc IEEE 2006;94(9):1652–64.

[4] Bergerman Marcel, Billingsley John, Reid John, van Henten Eldert. Robotics in agriculture and forestry. In: Springer handbook of robotics. Springer; 2016, p. 1463–92.

[5] de Wit Carlos Canudas, Siciliano Bruno, Bastin Georges. Theory of robot control. Springer Science & Business Media; 2012.

[6] Siciliano Bruno, Khatib Oussama, Kröger Torsten. Springer handbook of robotics, vol. 200. Springer; 2016.

[7] Kostarigka Artemis K, Doulgeri Zoe, Rovithakis George A. Prescribed performance tracking for flexible joint robots with unknown dynamics and variable elasticity. Automatica 2013;49(5):1137–47.

[8] Yang Chenguang, Huang Kunxia, Cheng Hong, Li Yanan, Su Chun-Yi. Haptic identification by ELM-controlled uncertain manipulator. IEEE Trans Syst Man Cybern Syst 2017;47(8):2398–409.

[9] Boussoffara Majdi, Ahmed Ikbel Ben Cheikh, Hajaiej Zied. Sliding mode controller design: stability analysis and tracking control for flexible joint manipulator. Rev Roumaine Sci Techn Sér Électrotech Énergétique 2021;66(3):161–7.

[10] Arkouli Z, Aivaliotis P, Makris S. Towards accurate robot modelling of flexible robotic manipulators. Procedia CIRP 2021;97:497–501.

[11] Nicosia Salvatore, Nicolo F, Lentini D. Dynamical control of industrial robots with elastic and dissipative joints. IFAC Proc Vol 1981;14(2):1933–40.

[12] Spong MW. Modeling and control of elastic joint robots. J Dyn Syst Meas Control 1987;109(4):310–9.

[13] Buondonno Gabriele, De Luca Alessandro. A recursive Newton-Euler algorithm for robots with elastic joints and its application to control. In: 2015 IEEE/RSJ International conference on intelligent robots and systems. IEEE; 2015, p. 5526–32.

[14] Farah Jacques, Chanal Hélène, Bouton Nicolas, Gagnol Vincent. A model-based control law for vibration reduction of serial robots with flexible joints. Mech Ind 2021;22:38.

[15] Bauchau Olivier A, Nemani Nishant. Modeling viscoelastic behavior in flexible multibody systems. Multibody Syst Dyn 2021;51(2):159–94.

[16] Baccelliere Lorenzo, Kashiri Navvab, Muratore Luca, Laurenzi Arturo, Kamedula Małgorzata, Margan Alessio, Cordasco Stefano, Malzahn Jörn, Tsagarakis Nikos G. Development of a human size and strength compliant bi-manual platform for realistic heavy manipulation tasks. In: 2017 IEEE/RSJ International conference on intelligent robots and systems. IEEE; 2017, p. 5594–601.

[17] Seweryn Karol, Grassmann Kamil, Ciesielska Monika, Rybus Tomasz, Turek Michal. Optimization of the robotic joint equipped with epicyloidal gear and direct drive for space applications. In: Proceedings of 15th European space mechanisms and tribology symposium. ESTEC; 2013, p. 3817–23.

[18] Guardiani Paolo, Ludovico Daniele, Pistone Alessandro, Abidi Haider, Zaplana Isiah, Lee Jinoh, Caldwell Darwin G, Canali Carlo. Design and analysis of a fully actuated cable-driven joint for hyper-redundant robots with optimal cable routing. J Mech Robot 2022;14(2):021006.

[19] Dong Xin, Raffles Mark, Cobos-Guzman Salvador, Axinte Dragos, Kell James. A novel continuum robot using twin-pivot compliant joints: design, modeling, and validation. J Mech Robot 2016;8(2):021010.

[20] Canali Carlo, Pistone Alessandro, Ludovico Daniele, Guardiani Paolo, Gagliardi Roberto, De Mari Casareto Dal Verme Lorenzo, Sofia Giuseppe, Caldwell Darwin G. Design of a novel long-reach cable-driven hyper-redundant snake-like manipulator for inspection and maintenance. Appl Sci 2022;12(7):3348.

[21] SPARC. Robotics 2020 Multi-Annual Roadmap. 2016, https://old.eu-robotics.net/cms/upload/topic_groups/H2020_Robotics_Multi-Annual_Roadmap_ICT-2017B.pdf. [Accessed 13 July 2023].

[22] Yeshmukhametov Azamat, Koganezawa Koichi, Yamamoto Yoshio. Design and kinematics of cable-driven continuum robot arm with universal joint backbone. In: 2018 IEEE International conference on robotics and biomimetics. IEEE; 2018, p. 2444–9.

[23] Endo Gen, Horigome Atsushi, Takata Atsushi. Super dragon: A 10-m-long-coupled tendon-driven articulated manipulator. IEEE Robot Autom Lett 2019;4(2):934–41.

[24] Horigome Atsushi, Endo Gen. Basic study for drive mechanism with synthetic fiber rope–investigation of strength reduction by bending and terminal fixation method. Adv Robot 2016;30(3):206–17.

[25] Horigome Atsushi, Endo Gen. Investigation of repetitive bending durability of synthetic fiber ropes. IEEE Robot Autom Lett 2018;3(3):1779–86.

[26] Uicker JJ. Dynamic force analysis of spatial linkages. J Appl Mech 1964;34(2):418–24.

[27] Bejczy Antal K. Robot arm dynamics and control. Technical report, National Aeronautics and Space Administration; 1974.

[28] Orin David E, McGhee RB, Vukobratović M, Hartoch G. Kinematic and kinetic analysis of open-chain linkages utilizing Newton-Euler methods. Math Biosci 1979;43(1–2):107–30.

[29] Hollerbach John M. A recursive lagrangian formulation of maniputator dynamics and a comparative study of dynamics formulation complexity. IEEE Trans Syst Man Cybern 1980;10(11):730–6.

[30] Silver William M. On the equivalence of Lagrangian and Newton-Euler dynamics for manipulators. Int J Robot Res 1982;1(2):60–70.

[31] Walker MW, Orin DE. Efficient dynamic computer simulation of robotic mechanisms. J Dyn Syst Meas Control 1982;104(3):205–11.

[32] Featherstone Roy. The calculation of robot dynamics using articulated-body inertias. Int J Robot Res 1983;2(1):13–30.

[33] Featherstone Roy, Orin David. Robot dynamics: equations and algorithms. In: Proceedings 2000 ICRA. Millennium conference. IEEE International conference on robotics and automation. symposia proceedings (Cat. No. 00CH37065), vol. 1. IEEE; 2000, p. 826–34.

[34] Zhao Yu, Wang Cong, Yu Xiaowen, Tomizuka Masayoshi. Complete dynamic modelling of flexible joint robots. In: Dynamic systems and control conference, vol. 57243. American Society of Mechanical Engineers; 2015, V001T18A003.

[35] Fichera Francesco, Grossard Mathieu. On the modeling and identification of stiffness in cable-based mechanical transmissions for robot manipulators. Mech Mach Theory 2017;108:176–90.

[36] Choi Sung-Hyun, Park Kyoung-Su. The integrated elasto-plastic cable modeling for cable driven parallel robots (CDPRs). In: 2017 17th International conference on control, automation and systems. IEEE; 2017, p. 420–2.

[37] Takata Atsushi, Endo Gen, Suzumori Koichi, Nabae Hiroyuki, Mizutani Yoshihiro, Suzuki Yoshiro. Modeling of synthetic fiber ropes and frequency response of long-distance cable–pulley system. IEEE Robot Autom Lett 2018;3(3):1743–50.

[38] Tomei Patrizio. A simple PD controller for robots with elastic joints. IEEE Trans Autom Control 1991;36(10):1208–13.

[39] Albu-Schäffer Alin, Ott Christian, Hirzinger Gerd. A unified passivity-based control framework for position, torque and impedance control of flexible joint robots. Int J Robot Res 2007;26(1):23–39.

[40] Caverly Ryan James, Forbes James Richard. Dynamic modeling and noncollocated control of a flexible planar cable-driven manipulator. IEEE Trans Robot 2014;30(6):1386–97.

[41] Wang Hesheng, Chen Weidong, Yu Xiaojin, Deng Tao, Wang Xiaozhou, Pfeifer Rolf. Visual servo control of cable-driven soft robotic manipulator. In: 2013 IEEE/RSJ International conference on intelligent robots and systems. IEEE; 2013, p. 57–62.

[42] Salimi Amirhossein, Ramezanifar Amin, Mohammadpour Javad, Grigoriadis Karolos. Gain-scheduling control of a cable-driven mri-compatible robotic platform for intracardiac interventions. In: 2013 American control conference. IEEE; 2013, p. 746–51.

[43] Wang Yaoyao, Yan Fei, Chen Jiawang, Ju Feng, Chen Bai. A new adaptive time-delay control scheme for cable-driven manipulators. IEEE Trans Ind Inf 2018;15(6):3469–81.

[44] Wang Yaoyao, Li Binbin, Yan Fei, Chen Bai. Practical adaptive fractional-order nonsingular terminal sliding mode control for a cable-driven manipulator. Internat J Robust Nonlinear Control 2019;29(5):1396–417.

[45] Wang Yaoyao, Zhang Rui, Ju Feng, Zhao Jinbo, Chen Bai, Wu Hongtao. A light cable-driven manipulator developed for aerial robots: Structure design and control research. Int J Adv Robot Syst 2020;17(3):1729881420926425.

[46] Sun Haining, Hou Senhao, Li Qunzhi, Tang Xiaoqiang. Research on the configuration of cable-driven parallel robots for vibration suppression of spatial flexible structures. Aerosp Sci Technol 2021;109:106434.

[47] Ludovico Daniele, Pistone Alessandro, De Mari Casareto Dal Verme Lorenzo, Guardiani Paolo, Caldwell Darwin G, Canali Carlo. Static elasticity compensation via recursive artificial neural network for long-reach cable-driven hyper-redundant manipulators. In: 2021 20th International conference on advanced robotics. IEEE; 2021, p. 1116–20.

[48] Johnson Charles Royal. Positive definite matrices. Amer Math Monthly 1970;77(3):259–64.

[49] Ludovico Daniele. Modelling and control of cable-driven hyper-redundant robots Doctor of Philosophy (Ph. D.), University of Genoa, Italy; 2021, https://hdl.handle.net/11567/1045135. [Accessed 13 July 2023].